J. Appl. Comput. Mech., 7(1) (2021) 345-354
DOI: 10.22055/JACM.2020.35564.2684

ISSN: 2383-4536
jacm.scu.ac.ir

Shahid Chamran University of Ahvaz

Journal of
Applied and Computational Mechanics

Research Paper

Buckling Analysis of Functionally Graded Shells under Mixed Boundary Conditions Subjected to Uniform Lateral Pressure

Abdullah Sofiyev[1], Fatih Dikmen[2]

[1] Department of Civil Engineering of Engineering Faculty, Suleyman Demirel University, 32260, Isparta, Turkey

[2] Student of Graduate School of Natural and Applied Sciences of Suleyman Demirel University, 32260, Isparta, Turkey

Received October 28 2020; Revised November 06 2020; Accepted for publication November 07 2020.
Corresponding author: A. Sofiyev (abdullahavey@sdu.edu.tr)

Abstract. In this study, the buckling problem of shells consisting of functionally graded materials (FGMs) under uniform compressive lateral pressure is solved at mixed boundary conditions. After creating the FGM models, the basic differential equations of FGM shells under compressive lateral pressure are derived within the scope of classical shell theory (CST). The basic differential equations are solved with the help of Galerkin method and the formula for the lateral buckling pressure is obtained. The minimum values of the lateral buckling pressure are found numerically by minimizing the obtained expression according to the numbers of transverse and longitudinal waves. The accuracy is confirmed by comparing the numerical values for the lateral buckling pressure of homogeneous and FGM shells with the results in the literature. The influences of FGM profiles and shell characteristics on the magnitudes of lateral buckling pressure are investigated in detail by performing specific numerical analyzes.

Keywords: Functionally graded materials, Shells, Uniform lateral pressure, Buckling pressure, Mixed boundary conditions

1. Introduction

The shells are used in a variety of engineering applications such as key components of missiles and spacecraft and other civil, mechanical and aerospace engineering applications. Studies on the buckling behavior of homogeneous isotropic shells under lateral pressure have been developed over the course of several decades. There are pioneering studies on the buckling of homogeneous isotropic shells under various boundary conditions and using different approaches [1-3].

The development of materials science has allowed new types of heterogeneous materials to be obtained artificially. This allows the shells to be formed from modern heterogeneous materials. One of such new generation heterogeneous materials are functionally graded materials (FGMs). FGMs consist of a mixture of two or more materials and whose properties continuously change from one surface to another. The properties of FGMs are unique and behave differently from the materials that comprise them [4]. FGMs are produced using physical or chemical vapor deposition (PVD / CVD), plasma sputtering, self-propagating high temperature synthesis (SHS), powder metallurgy technique, centrifuge casting method, solid free form technology, and other methods [5-9]. FGMs have aerospace and mechanical engineering, shipbuilding, automotive, medicine, sports, energy, sensors, optoelectronics, and various other application areas [10,11]. The advantages of FGMs over traditional composites have led to many studies in the field of improving their processing, production and processing properties) [12, 13].

Since FGMs constitute the basic structural elements used in spacecraft, aircraft, nuclear power plants and turbine blades, they are generally exposed to external pressures. In recent years, due to the increased interest in the design of engineering structures for FGMs with extraordinary properties, many studies have been carried out on the buckling analysis of structural elements with different shapes. One of the first studies on the buckling behavior of FGM structural plates and shells were proposed by Feldman and Aboudi [14] and Sofiyev [15], respectively. Following these studies, the natural vibration and stability behaviors of FGM cylindrical shells were analyzed by considering the effects of transverse shear and normal strains in Matsunaga [16]. A detailed review of the stability, vibration and buckling behavior of FGM composite members until 2009 can be found in the books of Shen [17]. Following these studies, extensive studies were conducted on the buckling of FGM shells with different shapes, and these studies were summarized in Sofiyev [18].

The rapid increase in the application of FGMs in modern technology has significantly increased the interest in investigating the buckling behavior of FGM shells with various boundary conditions under external pressures. The relevant studies have been continuing intensively since 2015 and have been investigated using various methods for different boundary conditions and loading conditions in various environment [19-28].

The number of publications dealing with the stability problem of shells under mixed boundary conditions is very limited due to the difficulties encountered during modeling and solution. Most of the publications on the solution of the buckling problem of FGM shells under mixed boundary conditions have been carried out by Sofiyev AH and his colleagues [29-33].

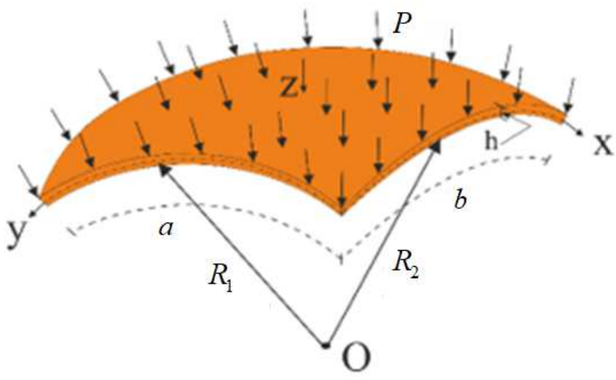

Fig. 1. FGM shell under external pressure, coordinate system and notations

In this study, the buckling behavior of FGM shells exposed to lateral external pressure under mixed boundary conditions is investigated. The mixed boundary conditions are as follows: One end of the FGM shells has a sleeve that prevents longitudinal displacement and rotation and the other end is freely support. The basic equations of FGM shells are derived using Donnell shell theory. To solve this problem, basic equations are solved by using new approximation functions and applying Galerkin method under mixed boundary conditions. The results in this study are confirmed by comparing results in the literature. The main purpose of the study under consideration is to investigate the influences of FGM profiles, volume fractions and geometrical characteristics on the lateral buckling pressure of cylindrical shells under mixed boundary conditions in detail.

2. Formulation of Problem

The double-curved shell composed of functionally graded material is subjected to uniform external pressure P and presented in Fig. 1. Suppose that the thickness of shell is h, the length is a, the width is b, and the radii of curvature are R_1 and R_2, respectively. The curvilinear coordinate system is located on the reference surface of the FGM shell. The x and y axes are oriented as shown in the Fig.1 and the z axis is in the normal direction to the surface where these two axes are, and it is directed towards the center of curvature.

The functionally graded material consists of a mixture of two different types of metal and ceramic materials. The general material properties of FGMs are shown with F, and their effective properties defined by the Voight model are as follows:

$$F = F_m V_m + F_c V_c \tag{1}$$

where V_m and V_c are the volume fraction functions of the metal and ceramic phases, respectively, providing the following equivalence:

$$V_m = 1 - V_c \tag{2}$$

The function of the volume fraction of the ceramic phase obeys the simple power rule [6, 15, 17]:

1. Power function

$$V_C = \left(\frac{z + h/2}{h}\right)^p, \ p \geq 0 \tag{3}$$

2. Inverse quadratic function:

$$V_c = 1 - \left(\frac{h/2 - z}{h}\right)^2 \tag{4}$$

Here p is called the volume fractional index and describes the grading of the material in the direction of thickness.

Considering the relations (1) and (2), namely the mixing rule, the effective properties of FGMs that forming shells are defined as follows [17]:

$$E_{fd}(\overline{z}) = E_m + (E_c - E_m)V_c, \quad \nu_{fd}(\overline{z}) = \nu_m + (\nu_c - \nu_m)V_c. \tag{5}$$

Here, E_m is the modulus of elasticity of metal, ν_m is the Poisson ratio of metal, E_c is the modulus of elasticity of ceramic and ν_c is the Poisson ratio of ceramic.

Detailed information about the formation, design and properties of various functional graded materials are presented by many researchers (See, [18]).

3. Derivation of Static Stability Equations

The constitutive equations of shells composed of functionally graded materials can be written in the framework of classical shell theory as follows [15, 17]:

$$\begin{bmatrix}\sigma_{xx}\\ \sigma_{yy}\\ \sigma_{xy}\end{bmatrix}=\begin{bmatrix}Y_{11\bar{z}} & Y_{12\bar{z}} & 0\\ Y_{12\bar{z}} & Y_{11\bar{z}} & 0\\ 0 & 0 & Y_{66\bar{z}}\end{bmatrix}\begin{bmatrix}e_{xx}^0-z\dfrac{\partial^2 w}{\partial x^2}\\ e_{yy}^0-z\dfrac{\partial^2 w}{\partial y^2}\\ \gamma_{xy}^0-2z\dfrac{\partial^2 w}{\partial x\partial y}\end{bmatrix} \tag{6}$$

where $\sigma_{xx},\sigma_{yy},\sigma_{xy}$ are stresses of shells made of FGMs, $e_{xx}^0, e_{xx}^0, \gamma_{xy}^0$ are the strains on the reference surface, w indicates the deflecting function and tends towards the center of curvature, and $Y_{ij\bar{z}}(,\ (i,j=1,2,6)$ is FGM properties that continuously change according to the dimensionless thickness coordinate $\bar{z}=z/h$ and is defined as follows:

$$Y_{11\bar{z}}=\frac{E_{fd}(\bar{z})}{1-\nu_{fd}^2(\bar{z})},\ Y_{12\bar{z}}=\nu_{fd}(\bar{z})\frac{E_{fd}(\bar{z})}{1-\nu_{fd}^2(\bar{z})},\ Y_{66\bar{z}}=\frac{E_{fd}(\bar{z})}{2\left(1+\nu_{fd}(\bar{z})\right)} \tag{7}$$

The force and moment components of circular shells made of functionally graded materials are obtained from the following integrals [1-3, 35]:

$$\begin{aligned}\left(N_{xx},N_{yy},N_{xy}\right)&=\int_{-h/2}^{+h/2}\left(\sigma_{xx},\sigma_{yy},\sigma_{xy}\right)dz\\ \left(M_{xx},M_{yy},M_{xy}\right)&=\int_{-h/2}^{+h/2}\left(z\sigma_{xx},z\sigma_{yy},z\sigma_{xy}\right)dz\end{aligned} \tag{8}$$

If the expression (9) is substituted in (10) and then integrated, the following equations are obtained for force and moment components of shells made of FGMs:

$$\begin{aligned}&N_{xx}=r_{10}\,e_{xx}^0+r_{20}\,e_{yy}^0-r_{11}\frac{\partial^2 w}{\partial x^2}-r_{21}\frac{\partial^2 w}{\partial y^2},N_{yy}=r_{20}\,e_{xx}^0+r_{10}\,e_{yy}^0-r_{21}\frac{\partial^2 w}{\partial x^2}-r_{11}\frac{\partial^2 w}{\partial y^2}\\ &N_{xy}=r_{60}\,\gamma_{xy}^0-2r_{61}\frac{\partial^2 w}{\partial x\partial y},\ M_{xx}=r_{11}\,e_{xx}^0+r_{21}\,e_{yy}^0-r_{12}\frac{\partial^2 w}{\partial x^2}-r_{22}\frac{\partial^2 w}{\partial y^2}\\ &M_{yy}=r_{21}\,e_{xx}^0+r_{11}\,e_{yy}^0-r_{22}\frac{\partial^2 w}{\partial x^2}-r_{12}\frac{\partial^2 w}{\partial y^2},\ M_{xy}=r_{61}\,\gamma_{xy}^0-2r_{62}\frac{\partial^2 w}{\partial x\partial y}\end{aligned} \tag{9}$$

Here, the following definitions apply:

$$\begin{aligned}&r_{1k}=\int_{-h/2}^{h/2}Y_{11\bar{z}}z^k\,dz,\ \ r_{2k}=\int_{-h/2}^{h/2}Y_{21\bar{z}}z^k\,dz,\ \ r_{6k}=\int_{-h/2}^{h/2}Y_{66\bar{z}}z^k\,dz,\\ &r_{1k}=\int_{-h/2}^{h/2}Y_{11\bar{z}}z^k\,dz,\ \ r_{2k}=\int_{-h/2}^{h/2}Y_{21\bar{z}}z^k\,dz,\ \ r_{6k}=\int_{-h/2}^{h/2}Y_{66\bar{z}}z^k\,dz,\ k=0,1,2\end{aligned} \tag{10}$$

With the Airy stress function Ψ, the force components can be expressed as follows [1-3, 35]:

$$\left(N_{xx},N_{yy},N_{xy}\right)=h\left(\frac{\partial^2\Psi}{\partial y^2},\frac{\partial^2\Psi}{\partial x^2},-\frac{\partial^2\Psi}{\partial x\partial y}\right) \tag{11}$$

The static stability equation of shallow shells composed of functionally graded materials is derived using the Hamiltonian principle as follows [2, 3]:

$$\frac{\partial^2 M_{xx}}{\partial x^2}+2\frac{\partial^2 M_{xy}}{\partial x\partial y}+\frac{\partial^2 M_{xy}}{\partial y^2}-P_L R_2\frac{\partial^2 w}{\partial y^2}+\frac{N_{xx}}{R_1}+\frac{N_{yy}}{R_2}=0 \tag{12}$$

$$\frac{\partial^2 e_{xx}^0}{\partial x^2}+\frac{\partial^2 e_{yy}^0}{\partial y^2}-\frac{\partial^2\gamma_{xy}^0}{\partial x\partial y}=-\frac{1}{R_2}\frac{\partial^2 w}{\partial x^2}-\frac{1}{R_1}\frac{\partial^2 w}{\partial y^2} \tag{13}$$

Using the Eqs. (9) and (11), the strains at the middle surface are expressed as the stress function, and the resulting expressions are substituted in the basic equations (12) and (13), after some operations they turn into the following form:

$$L_1(\Psi, w) \equiv h\left[c_2\frac{\partial^4\Psi}{\partial x^4} + 2(c_1 - c_5)\frac{\partial^4\Psi}{\partial x^2\partial y^2} + c_2\frac{\partial^4\phi}{\partial y^4} + \frac{1}{R_1}\frac{\partial^2\Psi}{\partial y^2} + \frac{1}{R_2}\frac{\partial^2\Psi}{\partial x^2}\right]$$
$$-P_L R\frac{\partial^2 w}{\partial y^2} - c_3\frac{\partial^4 w}{\partial x_1{}^4} - 2(c_4 + 2c_6)\frac{\partial^4 w}{\partial x_1{}^2\partial y^2} - c_4\frac{\partial^4 w}{\partial y^4} = 0 \tag{14}$$

$$L_2(\Psi, w) \equiv h\left[l_1\frac{\partial^4\Psi}{\partial y^4} + (2l_2 + l_5)\frac{\partial^4\Psi}{\partial x^2\partial y^2} + l_1\frac{\partial^4\Psi}{\partial x^4}\right] - l_3\frac{\partial^4 w}{\partial x^4}$$
$$-(2l_3 - l_6)\frac{\partial^4 w}{\partial x^2\partial y^2} - l_4\frac{\partial^4 w}{\partial y^4} + \frac{1}{R_2}\frac{\partial^2 w}{\partial x^2} + \frac{1}{R_1}\frac{\partial^2 w}{\partial y^2} = 0 \tag{15}$$

Here, the following definitions apply:

$$c_1 = r_{11}l_1 + r_{21}l_2,\ c_2 = r_{11}l_2 + r_{21}l_1,\ c_3 = r_{11}l_3 + r_{21}l_4 + r_{12},\ c_4 = r_{11}l_4 + r_{21}l_3 + r_{22},$$
$$c_5 = r_{61}l_5,\ c_6 = r_{61}l_6 + r_{62},\ l_1 = r_{10}\mu,\ l_2 = -r_{20}\mu,\ l_3 = (r_{20}r_{21} - r_{11}r_{10})\mu,$$
$$l_4 = (r_{20}r_{11} - r_{21}r_{10})\mu,\ l_5 = \frac{1}{r_{60}},\ l_6 = -\frac{2r_{61}}{r_{60}},\ \mu = \frac{1}{r_{10}r_{10} - r_{20}r_{20}} \tag{16}$$

The Eqs. (14) and (15) are static stability and deformation compatibility equations of shells made of FGMs and can be used in stability problems.

In a particular case, taking into account $R_2 = R,\ R_1 \to \infty$ in the Eqs. (15) and (16), the following basic equations for FGM cylindrical shells are obtained:

$$\bar{L}_1(\Psi, w) \equiv h\left[c_2\frac{\partial^4\Psi}{\partial x^4} + 2(c_1 - c_5)\frac{\partial^4\Psi}{\partial x^2\partial y^2} + c_2\frac{\partial^4\phi}{\partial y^4} + \frac{1}{R}\frac{\partial^2\Psi}{\partial x^2}\right]$$
$$-P_L R\frac{\partial^2 w}{\partial y^2} - c_3\frac{\partial^4 w}{\partial x^4} - 2(c_4 + 2c_6)\frac{\partial^4 w}{\partial x^2\partial y^2} - c_4\frac{\partial^4 w}{\partial y^4} = 0 \tag{17}$$

$$\bar{L}_2(\Psi, w) \equiv h\left[l_1\frac{\partial^4\Psi}{\partial y^4} + (2l_2 + l_5)\frac{\partial^4\Psi}{\partial x^2\partial y^2} + l_1\frac{\partial^4\Psi}{\partial x^4}\right] - l_3\frac{\partial^4 w}{\partial x^4}$$
$$-(2l_3 - l_6)\frac{\partial^4 w}{\partial x^2\partial y^2} - l_4\frac{\partial^4 w}{\partial y^4} + \frac{1}{R}\frac{\partial^2 w}{\partial x^2} = 0 \tag{18}$$

As $R_1 \to \infty$ the double curvature shell transforms into the cylindrical shell shown in Figure 2. Here a and R_2 are denoted by L and R, and the external pressure P converted the lateral pressure P_L (see, Fig 2.).

The system of differential equations (17) and (18) can be used in the stability problems of FGM cylindrical shells.

4. Solution of Stability Equations

One end of the functionally graded cylindrical shell uses a clutch that prevents its longitudinal displacement and rotation, and the other end is simply supported. The mathematical model of mixed boundary conditions is defined as follows [31, 34]:

$$w = \frac{\partial^2 w}{\partial x^2} = 0 \quad \text{and} \quad u = \frac{\partial^2 w}{\partial x^2} = 0 \quad \text{for } x = 0 \quad \text{and} \quad x = L \tag{19}$$

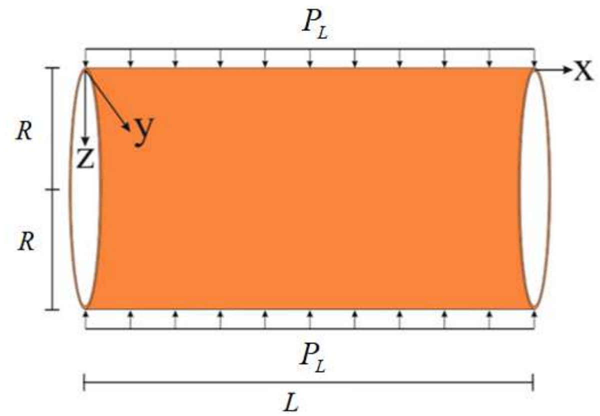

Fig. 2. FGM cylindrical shell under lateral pressure, coordinate system and notations

The solution of the stability and deformation compatibility equations of the FGM cylindrical shells, which satisfies the boundary conditions (17), is sought as the following functions:

$$w = w_1 \sin\left(\frac{m_1 x}{2}\right)\cos(n_1 y),\ \Psi = \Psi_1 \sin\left(\frac{m_1 x}{2}\right)\cos(n_1 y) \tag{20}$$

where w_1 and Ψ_1 are amplitudes, $m_1 = m\pi / L$, $m = 1,3,5,...$ and $n_1 = n / R$, the number of waves in the x direction is m and the number of waves in the y direction is n.

Let's apply the Galerkin method to the basic equations (14) and (15):

$$\int_0^{2\pi R}\int_0^{L} \bar{L}_1(\Psi, w)\sin\left(\frac{m_1 x}{2}\right)\cos(n_1 y)dxdy = 0 \tag{21}$$

$$\int_0^{2\pi R}\int_0^{L} \bar{L}_2(\Psi, w)\sin\left(\frac{m_1 x}{2}\right)\cos(n_1 y)dxdy = 0 \tag{22}$$

As the Eq. (20) are substituted into Eqs. (21) and (22) and after integrating, the parameter Ψ_1 is eliminated from the two resulting algebraic equations, the following equation is obtained for the lateral buckling pressure (LBP) of FGM shells:

$$P_L^{buc} = \frac{1}{R^5 n_1^{\,2}}\left\{c_3 m_2^{\,4} + 4c_6 m_2^{\,2} n^2 + 16 c_3 n^4 + \left[4m_2^{\,2}R - c_2 m_2^{\,4} - 8(c_1 - c_5)m_2^{\,2}n^2 - 16c_2 n^4\right] \times \frac{\left[4m_2^{\,2}R + l_4 m_2^{\,4} + 8(l_3 - l_6)m_2^{\,2}n^2 + 16 l_4 n^4\right]}{l_1 m_2^{\,4} + 4 l_5 m_2^{\,2} n^2 + 16 l_1 n^4}\right\} \tag{23}$$

where

$$m_2 = \frac{m\pi R}{L} \tag{24}$$

To find the minimum value of the lateral buckling pressure, the expression (23) is minimized with respect to wave numbers (m, n).

5. Results and Discussion

5.1. Comparisons

Under this heading, the numerical calculations have been made by using the expression (23) obtaining for lateral buckling pressure of FGM cylindrical shells under mixed boundary conditions and the results are compared with the results in the literature. In this comparison, the values of the lateral buckling pressure of the pure metal cylindrical shell under mixed boundary conditions are compared with the results of Refs. [31] and [34]. In the study [31] shear deformation theory is used. Ref. [34] used the following expression for the lateral buckling pressure:

$$P_{LAS}^{buc} = \frac{E_m h}{(n^2-1)R}\left[\frac{h^2}{12(1-\nu_m^2)}\frac{m_2^{\,4} + 8m_2^{\,2}n^2 + 16(n^2-1)^2}{16R^2} + \frac{m_2^{\,4}}{(m_2^{\,2}+4n^2)^2}\right] \tag{25}$$

The material properties and geometric characteristics that make up the cylindrical shell are as follows: $E_m = 1.93\times 10^{11}$ Pa, $\nu_m = 0.3$ and $h = 0.01$m, $L/R = 3$, respectively. Where E_m and ν_m are Young's modulus and Poisson ratio of the homogeneous isotropic material, respectively. The minimum values of the lateral buckling pressure correspond to the case where the number of longitudinal waves is equal to one, i.e., m = 1.

Numerical calculations were carried out for different radius-thickness ratios (R/h) of the lateral buckling pressure for the cylindrical shell formed from nickel and presented in Table 1. From Table 1, it can be seen that our results for the lateral buckling pressure and the corresponding n_{cr} wave number for the homogeneous cylindrical shell are in good agreement with the results of Refs. [31] and [34].

5.2. Modeling of FGM Features

The shell is formed from FGMs and its effective properties are determined using the following equation [36]:

Table 1. Comparison of the results of this study of the lateral buckling compressive load with other results.

	P_L^{buc} (Pa) , (n_{cr})		
R/h	Ref. [34]	Ref. [31]	Present study
100	2.9526(11)	2.9633(11)	2.9634(11)
125	1.6890(12)	1.6945(12)	1.6952(12)
150	1.0836(13)	1.0873 (13)	1.0876 (13)
200	0.5260(14)	0.5308(14)	0.5303(14)

$$F_{fd} = F_0 F_{-1} T^{-1} + 1 + F_0 F_1 T + F_0 F_2 T^2 + F_0 F_3 T^3 \tag{26}$$

Here, F_i, $i = -1,0,1,2,3$, are sub-index changes from -1 to 3 in steps, and T (K) are the specific temperature coefficients for the components.

In the numerical analysis part, two different material types such as FGM_1 and FGM_2 are discussed. Silicon nitrate (Si_3N_4) and zirconium oxide (ZrO_2) ceramic types are mixed with nickel (Ni) and stainless steel (SUS304) metal types, respectively, to form FGMs. FGM_1 type cylindrical shell is mixture Si_3N_4/Ni and FGM_2 cylindrical shell is mixture ZrO_2/SUS304. FGMs constants are taken from book of the Shen [17]. The Young's modulus and Poisson's ratios of FGM_1 and FGM_2 are expressed as a function of temperature as follows:

$$\begin{aligned}
&FGM_1: \\
&E_{Si_3N_4} = 3.4843\times10^{11}(1-3.07\times10^{-4}T+2.16\times10^{-7}T^2-8.946\times10^{-11}T^3) \\
&\qquad = 3.22271\times10^{11}(\mathrm{Pa}) \\
&E_{Ni} = 2.2395\times10^{11}(1-2.794\times10^{-4}T-3.998\times10^{-9}T^2) = 2.05098\times10^{11}(\mathrm{Pa}) \\
&\nu_{Si_3N_4} = 0.24, \qquad \nu_{Ni} = 0.31
\end{aligned} \tag{27}$$

$$\begin{aligned}
&FGM_2: \\
&E_{ZrO_2} = 2.4427\times10^{11}(1-1.371\times10^{-3}T+1.214\times10^{-6}T^2-3.681\times10^{-10}T^3) \\
&\qquad = 1.68063\times10^{11}(\mathrm{Pa}) \\
&E_{Sus304} = 2.0104\times10^{11}(1+3.079\times10^{-4}T-6.534\times10^{-7}T^2) = 2.07788\times10^{11}(\mathrm{Pa}) \\
&\nu_{ZrO_2} = 0.2882(1+1.133\times10^{-4}T) = 0.297996 \\
&\nu_{Sus304} = 0.3262(1-2.002\times10^{-7}T+3.797\times10^{-7}T^2) = 0.317756
\end{aligned} \tag{28}$$

In Figs. 3-5, three dimensional changes of dimensionless Young's modulus $E_{fd}(\overline{z})$ according to dimensionless thickness coordinate $\overline{z}$ are presented for different volume fractions of shells composed of a) FGM_1 or Si_3N_4 / Ni and b) FGM_2 or ZrO_2/SUS304. In Figs. 3-5, the symbols $E_{1fd}(\overline{z}) = E_{fd}(\overline{z}) / E_m$, $\overline{z} = z/h$ and $\overline{x} = x/L$ are used on the axes.

As the volume fraction of shells with type a) FGM_1 and b) FGM_2 changes linearly, by writing $p=1$ and $p=2$ in the expression $E_{1fd} = 1 + ((z+h/2)/h)^p (E_c/E_m - 1)$, three dimensional distributions of the dimensionless Young's modulus depending on the $\overline{z}$ are presented in Figs. 3 and 4.

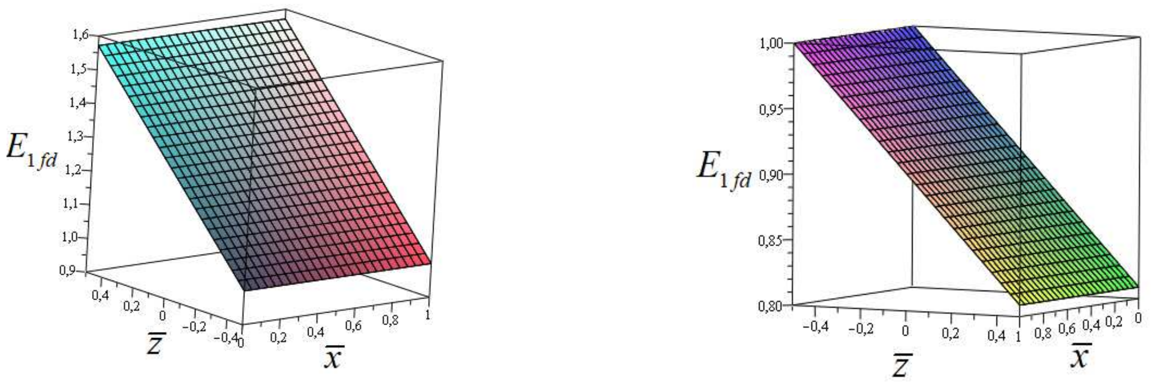

(a) (b)

Fig. 3. Distribution of Young's modulus of (a) FGM_1 and (b) FGM_2 types of shells depending on the $\overline{z}$ for $p=1$.

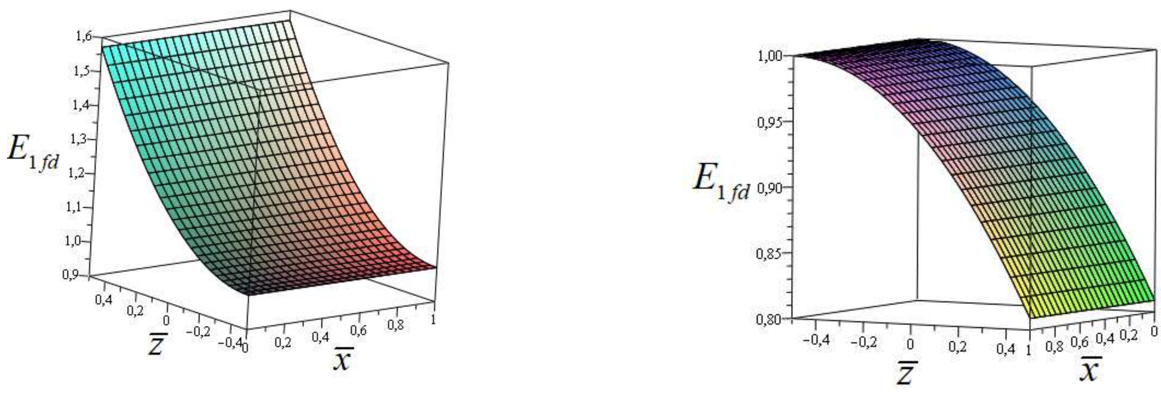

(a) (b)

Fig. 4. Distribution of Young's modulus of (a) FGM_1 and (b) FGM_2 types of shells depending on the $\overline{z}$ for $p=2$.

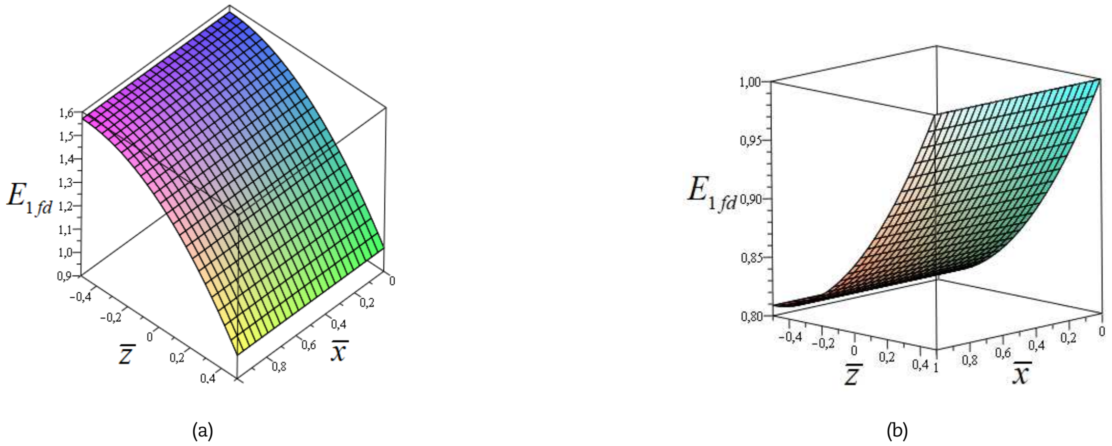

Fig. 5. Distribution of Young's modulus of (a) FGM_1 and (b) FGM_2 types of shells depending on the $\overline{z}$ for inverse quadratic case.

As the volume fraction of shells with types a) FGM_1 and b) FGM_2 changes inverse quadratic, i.e., $E_{1fd} = 1 + (E_c / E_m - 1)((h/2 - z)/h)^2$, three dimensional distributions of the dimensionless Young's modulus depending on the $\overline{z}$ are presented in Fig. 5.

5.3. Specific Analysis for Lateral Buckling Pressure of FGM Cylindrical Shells Under Mixed Boundary Conditions

The variation of the lateral buckling pressure of FGM_1 and FGM_2 types of cylindrical shells is presented in Table 2, Figs. 6 and 7 with $L/R = 2$. As can be seen from Table 2, Figs. 6 and 7, the values of lateral buckling pressure of pure metal (Ni and SUS304), pure ceramic (Si_3N_4 and ZrO_2) and FGM_i (i=1,2) shells decrease, while wave numbers remain constant for $R/h > 125$ and increases for other cases.

As the FGM_i (i = 1,2) shells are compared with the pure metal (Ni or SUS304) shells, the influences of FGM_i (i = 1,2) profiles on the LBP decrease weakly due to the increase of the R/h. In addition, the largest influence of FGM_i occurs in the inverse quadratic case, while the little effect occurs in the cubic case.

For instance, the effects of FGM_1 on the P_L^{buc} decrease from (+34.79%) to (+33.72%) at the inverse quadratic case and from (+17.89%) to (+17.44%) at the case of $p = 3$, respectively, due to R/h increases from 100 to 200. When the volume fraction of FGM_1 change as a power function are compared among themselves, the largest effect of FGM_1 profile on the P_L^{buc} occurs in the case of $p = 1$, while the smallest influence of FGM_1 on the lateral buckling pressure occurs in the case of $p = 3$. For example, the effects of FGM_1 on the LBP are (+26.74%), (+20.93%) and (+17.44%) at linear, quadratic and cubic cases, respectively for $R/h = 200$.

The effect of FGM_2 on the P_L^{buc} decreases from (-%12.13) to (-%11.49) at the inverse quadratic case and from (-%5.87) to (-%5.75) at the case of $p = 3$, respectively, due to R/h increases from 100 to 200. When the volume fraction of FGM_2 change as a power function are compared among themselves, the largest FGM_2 effect occurs in the case of $p = 1$, while the smallest influence of FGM_2 on the lateral buckling pressure occurs in the case of $p = 3$. For example, the effects of FGM_2 profiles on the LBP are (-%9.59), (-%7.24) and (-%5.87) for $p = 1, 2$ and $p = 3$, respectively with $R/h = 200$.

As the FGM_i (i = 1,2) shells are compared with the pure ceramic (Si_3N_4 or ZrO_2) shells, respectively, the influences of FGM_i (i = 1,2) profiles on the LBP decrease weakly with the increasing of R/h and the largest influence of FGM_i occurs at the cubic profile, while the little effect occurs in the inverse quadratic case.

For example, the influences of FGM_1 on the P_L^{buc} decrease from (-11.83%) to (-12.21%) for the inverse quadratic case and from (-22.89%) to (-22.9%) for $p = 3$, respectively, as the R/h increases from 100 to 200. When the volume fraction of FGM_1 profile change as a power function and are compared among themselves, the largest influences of FGM_1 occurs at $p = 3$, while the smallest influence of FGM_1 on the on the P_L^{buc} occurs at $p = 1$. For example, the effects of FGM_1 on the LBP are (-%16.25), (-%20.68) and (-%22.89) for linear, quadratic and cubic profiles, respectively for $R/h = 200$.

The influence of FGM_2 profile on the LBP increases from (+9.51%) to (+10%) at the inverse quadratic case and decreases from (+%17.32) to (+%17.14) for p = 3, respectively, as the R/h increases from 100 to 200. When the volume fraction of FGM_2 change as a power function are compared among themselves, the largest influence of FGM_2 profiles occurs for $p = 3$, while the smallest influence of FGM_2 on the LBP occurs for $p = 1$.

Table 2. Distribution of P_L^{buc} (MPa) and (n_{cr}) for FGM_1 and FGM_2 cylindrical shells depending on R/h ratio ($L/R = 2$)

P_L^{buc} (MPa), (n_{cr})						
R/h	Ni	FGM_1				Si_3N_4
		Liner	Quad.	Cubic	Inv. quad.	
100	0.503(4)	0.644(4)	0.610(4)	0.593(4)	0.678(4)	0.769(4)
125	0.292(5)	0.369(5)	0.352(5)	0.344(5)	0.386(5)	0.443(5)
150	0.179(5)	0.226(5)	0.216(5)	0.210(5)	0.237(5)	0.271(5)
175	0.120(5)	0.152(5)	0.145(5)	0.141(5)	0.160(5)	0.182(5)
200	0.086(5)	0.109(5)	0.104(5)	0.101(5)	0.115(5)	0.131(5)
R/h	SUS304	FGM_2				ZrO_2
		Liner	Quad.	Cubic	Inv. quad.	
100	0.511(4)	0.462(4)	0.474(4)	0.481(4)	0.449(4)	0.410(4)
125	0.297(5)	0.268(5)	0.274(5)	0.277(5)	0.261(5)	0.238(5)
150	0.182(5)	0.164(5)	0.168(5)	0.170(5)	0.160(5)	0.146(5)
175	0.122(5)	0.110(5)	0.113(5)	0.114(5)	0.107(5)	0.098(5)
200	0.087(5)	0.079(5)	0.081(5)	0.082(5)	0.077(5)	0.070(5)

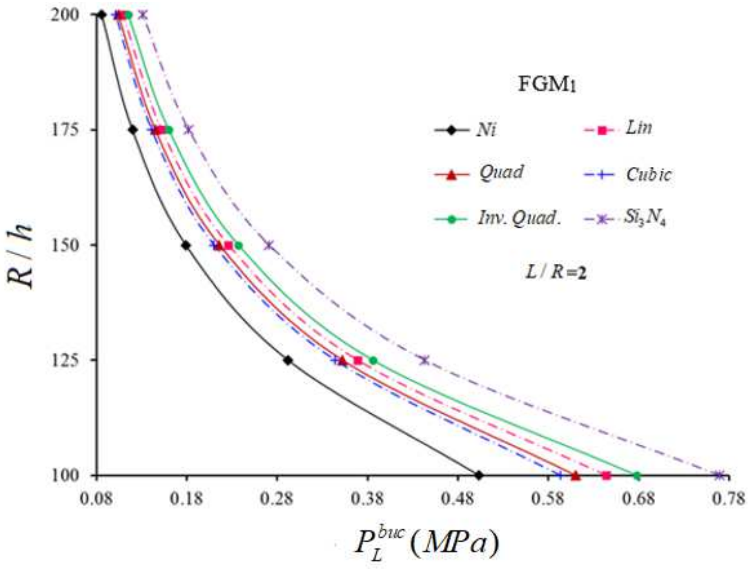

Fig. 6. Distribution of P_L^{buc}(MPa) for FGM$_1$ cylindrical shells depending on R / h ratio (L / R = 2)

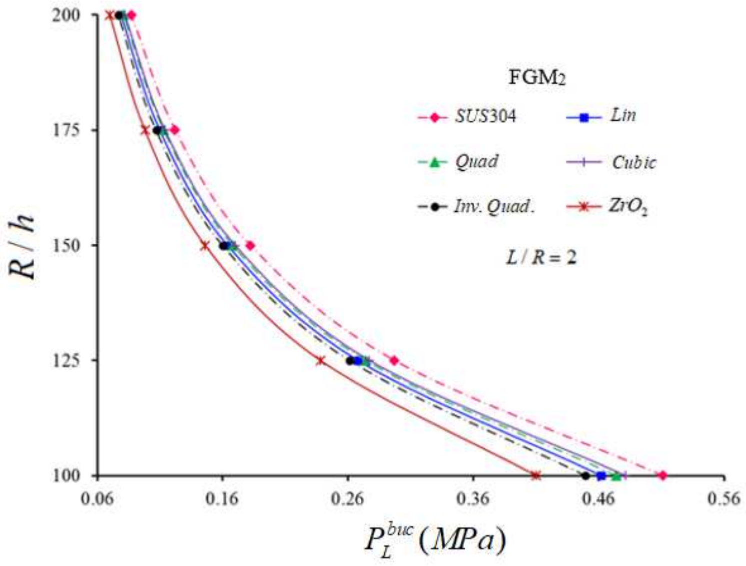

Fig. 7. Distribution of P_L^{buc}(MPa) for FGM$_2$ cylindrical shells depending on R / h ratio (L / R = 2)

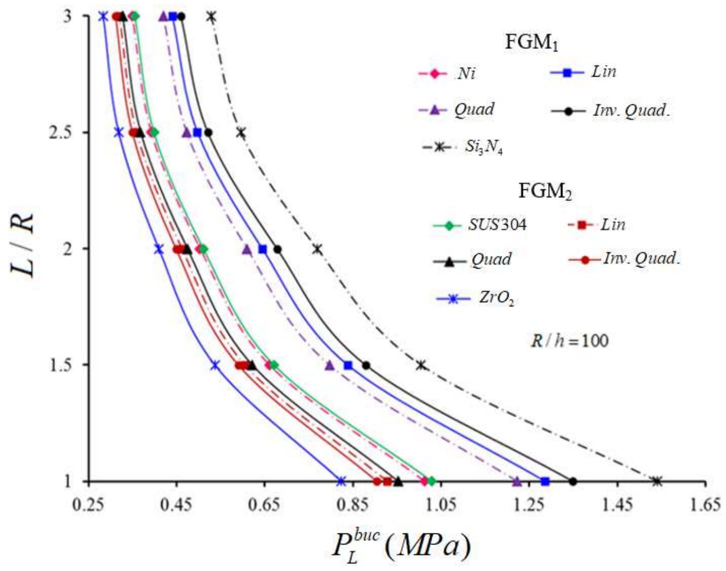

Fig. 8. Distribution of P_L^{buc}(MPa) for FGM$_1$ and FGM$_2$ cylindrical shells depending on the L / R ratio (L / R = 2)

The variation of the P_L^{buc} for cylindrical shells that formed from FGM_1 and FGM_2 profiles versus the L/R ratio is presented in Fig. 7 with $R/h = 100$. As can be seen from Fig. 7, the magnitudes of the lateral buckling pressure decrease due to the increase of L/R ratio at pure metal (Ni and SUS304), pure ceramic (Si_3N_4 and ZrO2), FGM_1 and FGM_2 shells. It is determined that the lateral buckling pressure values for the SUS304 shell are greater than the values for the nickel shells, whereas the values of LBP for ZrO_2 shells is smaller than the values for Si_3N_4 shells at $L/R = 1$. However, the magnitudes of the LBP of FGM_1 cylindrical shells are higher than the values of the FGM_2 cylindrical shells.

When the magnitudes of LBP for FGM_1 and FGM_2 cylindrical shells are compared with the pure metal cylindrical shells, the largest effect of FGM_1 occurs at the inverse quadratic case (+33.30%), whereas the smallest FGM_2 effect occurs at $p = 2$ profile (-7.48%), as the $L/R = 1$. As the values of on the P_L^{buc} for FGM_1 and FGM_2 shells are compared with pure ceramic shells, the greatest FGM_1 effect occurs for the quadratic profile of the cylindrical shell (-20.60%) at $L/R = 3$, while the smallest FGM_2 effect occurs in the inverse quadratic profile of cylindrical shell (+9.71%) at $L/R = 1$.

6. Conclusion

In this study, the buckling problem of cylindrical shells composed of FGMs under uniform lateral pressure is solved under mixed boundary conditions. After the FGM models are created, the basic differential equations of the FGM cylindrical shells under the uniform lateral pressure in the framework of CST are obtained. The basic differential equations are solved with the help of Galerkin method and the formula for lateral buckling pressure is found. The minimum values of the lateral buckling pressure are found numerically by minimizing the obtained expression according to the number of transverse and longitudinal waves. The numerical values obtained for the lateral buckling pressure for homogeneous and FGM shells are compared with other results in the literature to confirm their accuracy. In the analysis section, the effects of FGMs on the magnitudes of the lateral buckling pressure are tested with new and unique numerical samples for FGM_1 and FGM_2 profiles.

The generalizations of numerical results in the thesis are presented below:

a.) The magnitudes of lateral buckling pressure for FGM_1 shells are greater than the values for FGM_2 type shells.

b.) The magnitudes of lateral buckling pressure of FGM_1 and FGM_2 shells decrease due to the increase of the L/R ratio, while the wave numbers remain constant for $L/R > 2$, and decrease for other cases.

c.) The LBP of the FGM_1 and FGM_2 shells decrease due to the increases of the R/h ratio, while the wave numbers remain constant for $R/h > 125$ and increase for other cases.

d.) As the magnitudes of LBP for FGM_1 and FGM_2 cylindrical shells are compared with metal cylindrical shells, the largest effect of FGM_1 profile is obtained in the inverse quadratic case, while the smallest effect of FGM_2 is obtained at the quadratic profile of the shell, as $L/R = 1$.

e.) When the values of the LBP for FGM_1 and FGM_2 shells are compared with ceramic shells, the largest effect of FGM_1 is occur at $L/R = 3$ for the quadratic profile, while the smallest effect of FGM_2 occurs for the inverse quadratic profile, as $L/R = 1$.

f.) When the values LBP of the FGM_1 and FGM_2 cylindrical shells are compared with those of the metal cylindrical shells, the largest effect of FGM_1 occurs for the inverse quadratic profile at $R/h = 100$, and the smallest effect of FGM_2 on the LBP is occur for the quadratic profile at $R/h = 200$.

Author Contributions

A. Sofiyev planned the Formal analysis, Investigation, Validation, Writing—Original Draft and Writing—Review & Editing; F. Dikmen conducted Investigation, Validation, Writing—Original Draft and Writing—Review & Editing. The manuscript was written through the contribution of all authors. All authors discussed the results, reviewed, and approved the final version of the manuscript.

Conflict of Interest

The authors declared no potential conflicts of interest with respect to the research, authorship, and publication of this article.

Funding

The authors received no financial support for the research, authorship, and publication of this article.

Reference

[1] Sobel, L.H., Effects of boundary conditions on the stability of cylinders subject to lateral and axial pressures, *American Institute of Aeronautics and Astronautics (AIAA) Journal*, 2(8), 1964, 1437-1440.

[2] Volmir, A.S., *Stability of elastic systems*. Nauka, Moscow. English Translation: Foreign Tech. Division, Air Force Systems Command. Wright-Patterson Air Force Base, Ohio, AD628508, 1967.

[3] Vinson, J.R., *The behavior of thin walled structures: beams, plates, and shells*, Hardback Mechanics of Surface Structure, 1989.

[4] Koizumi, M., Niino, M., *Overview of FGM research in Japan*, Cambridge University, 20(1), 1995, 19-21.

[5] Zuiker, J.R., Functionally graded materials: choice of micromechanics model and limitations in property variation, *Composites Engineering*, 5(7), 1995, 807-819.

[6] Nogata, F., Takahashi, H., Intelligent functionally graded material: Bamboo, *Composites Engineering*, 5(7), 1995, 743-751.

[7] Giannakopoulos, A. E., Suresh, S., Indentation of solids with gradients in elastic properties: Part I. point force solution, *International Journal of Solids and Structures*, 34, 1997, 2357–2392.

[8] Kawasaki, A., Watanabe, R. Concept and P/M fabrication of functionally gradient materials, *Ceramic International*, 23(1), 1997, 73–83.

[9] Yu J., Kidane, A., Modeling functionally graded materials containing multiple heterogeneities, *Acta Mechanica*, 225, 2014, 1931-1943.

[10] Kawasaki, A., Kumakawa, A., Niino, M., *Multiscale, multifunctional and functionally graded materials*, Trans Tech Publication, 2010.

[11] Elishakoff, I., Panderas, D., Gentilini, C., *Mechanics of functionally graded material structures*, World Scientific Publishing, 2015.

[12] Ichikawa, K., *Functionally graded materials in the 21st century: A workshop on trends and forecasts*, Springer Science & Business Media, New York, 2013.

[13] Bui, T.Q., Lich, L.V., Singh, I.V., *Advances in mechanical problems of functionally graded materials and structures*, Materials, MDPI, Basel, 2019.

[14] Feldman, E., Aboudi, J., Buckling analysis of functionally graded plates subjected to uniaxial loading, *Composite Structures*, 38, 1997, 29-36.

[15] Sofiyev, A.H., Dynamic buckling of functionally graded cylindrical thin shells under non-periodic impulsive loading, *Acta Mechanica*, 165, 2003,151–163.

[16] Matsunaga, H., Free vibration and stability of functionally graded circular cylindrical shells according to a 2d higher-order deformation theory, *Composite Structures*, 88, 2009, 519–531.

[17] Shen, H.S., *Functionally graded materials, nonlinear analysis of plates and shells*, CRC Press, Florida, 2009.
[18] Sofiyev, A.H., Review of research on the vibration and buckling of the FGM conical shells, *Composite Structures*, 211, 2019, 301-317.
[19] Zhang, Y., Huang, H., Han, Q., Buckling of elastoplastic functionally graded cylindrical shells under combined compression and pressure, *Composites Part B: Engineering*, 69, 2015, 120-126.
[20] Sun, J., Xu, X., Lim, C., Qiao, W., Accurate buckling analysis for shear deformable FGM cylindrical shells under axial compression and thermal loads, *Composite Structures*, 123, 2015, 246-256.
[21] Kar, V.R., Panda, S.K., Post-buckling behavior of shear deformable functionally graded curved shell panel under edge compression, *International Journal of Mechanical Sciences*, 115, 2016, 318-324.
[22] Seifi, R., Avatefi, M., Effects of internal pressure on bending buckling of imperfect functionally graded thin cylinders, *Composite Structures*, 157, 2016, 12-24.
[23] Huang, H., Zhang, Y., Han, Q., Inelastic buckling of FGM cylindrical shells subjected to combined axial and torsional loads, *International Journal of Structural Stability and Dynamics*, 17(9), 2017, 1771010.
[24] Wang, Z., Han, Q., Nash, D.H., Liu, P., Hu, D., Investigation of imperfect effect on thermal buckling of cylindrical shell with FGM coating, *European Journal of Mechanics-A/Solids*, 69, 2018, 221-230.
[25] Jena, S.K., Chakraverty, S., Malikan, M., Application of shifted Chebyshev polynomial-based Rayleigh–Ritz method and Navier's technique for vibration analysis of a functionally graded porous beam embedded in Kerr foundation, *Engineering with Computers*, 2020, 1-21.
[26] Jena, S.K., Chakraverty, S., Malikan, M., Sedighi H.M., Implementation of Hermite–Ritz method and Navier's technique for vibration of functionally graded porous nanobeam embedded in Winkler–Pasternak elastic foundation using bi-Helmholtz nonlocal elasticity, *Journal of Mechanics of Materials and Structures*, 15(3), 2020, 405-434.
[27] Jena, S.K., Chakraverty, S., Malikan, M., Tornabene, F., Stability analysis of single-walled carbon nanotubes embedded in winkler foundation placed in a thermal environment considering the surface effect using a new refined beam theory, *Mechanics Based Design of Structures and Machines*, 2020, 1-15 (in press).
[28] Ghatage, P.S., Kar, V.R., Sudhagar, P.E., On the numerical modelling and analysis of multi-directional functionally graded composite structures: a review, *Composite Structures*, 236, 2020, 111837.
[29] Babaei, H., Jabbari, M., Eslami, M.R., The effect of porosity on elastic stability of toroidal shell segments made of saturated porous functionally graded materials, *Journal of Pressure Vessel Technology*, 143(3), 2021, 031501.
[30] Sofiyev, A.H., Kuruoglu, N., On the solution of the buckling problem of functionally graded truncated conical shells with mixed boundary conditions, *Composite Structures*, 123, 2015, 282-291.
[31] Jin, G., Ye, T., Wang, X., Miao, X., A unified solution for the vibration analysis of FGM doubly-curved shells of revolution with arbitrary boundary conditions, *Composites Part B: Engineering*, 89, 2016, 230-252.
[32] Sofiyev, A.H., Hui, D., On the vibration and stability of FGM cylindrical shells under external pressures with mixed boundary conditions by using FOSDT, *Thin-Walled Structures*, 134, 2019, 419-427.
[33] Sofiyev, A.H., The buckling and vibration analysis of coating-FGM-substrate conical shells under hydrostatic pressure with mixed boundary conditions, *Composite Structures*, 209, 2019, 686-693.
[34] Bayramov, R.P., Sofiyev, A.H., Dikmen, F., *Stability of layered cylindrical shells with FGM interlayer subjected to combined load under mixed boundary conditions*, Proc. 3th International Conference on Engineering Technologies (ICENTE'19), 462-465, 2019, Konya, Turkey, 25-27 October, 2019.
[35] Agenosov, L.G., Sachenkov, A.V., *Stability and free vibration of thin circular cylindrical and conical shells with different boundary conditions. Research on the theory of plates and shells*, Kazan State University, Kazan, USSR, 2, 1964, 111–126 (in Russian).
[36] Eslami, M.R., *Buckling and postbuckling of beams, plates and shells*, Springer, Switzerland, 2018.
[37] Touloukian, Y.S., *Thermo physical properties of high temperature solid materials*, McMillan, New York, 1967.

ORCID iD

Abdullah Sofiyev https://orcid.org/0000-0001-7678-6351
Fatih Dikmen https://orcid.org/0000-0001-8136-046X

How to cite this article: Sofiyev A., Dikmen F. Buckling Analysis of Functionally Graded Shells under Mixed Boundary Conditions Subjected to Uniform Lateral Pressure, *J. Appl. Comput. Mech.*, 7(1), 2021, 345–354. https://doi.org/10.22055/JACM.2020.35564.2684